

Effects of temperature and ammonia flow rate on the chemical vapour deposition growth of nitrogen-doped graphene†

A. A. Koós,^{ab} A. T. Murdock,^a P. Nemes-Incze,^b R. J. Nicholls,^a A. J. Pollard,^c S. J. Spencer,^c A. G. Shard,^c D. Roy,^c L. P. Biró^b and N. Grobert*^a

We doped graphene *in situ* during synthesis from methane and ammonia on copper in a low-pressure chemical vapour deposition system, and investigated the effect of the synthesis temperature and ammonia concentration on the growth. Raman and X-ray photoelectron spectroscopy was used to investigate the quality and nitrogen content of the graphene and demonstrated that decreasing the synthesis temperature and increasing the ammonia flow rate results in an increase in the concentration of nitrogen dopants up to ca. 2.1% overall. However, concurrent SEM studies demonstrate that decreasing both the growth temperature from 1000 to 900 °C and increasing the N/C precursor ratio from 1/50 to 1/10 significantly decreased the growth rate by a factor of six overall. Using scanning tunneling microscopy we show that the nitrogen was incorporated mainly in substitutional configuration, while current imaging tunneling spectroscopy showed that the effect of the nitrogen on the density of states was visible only over a few atom distances.

Received 16th May 2014,
Accepted 30th July 2014

DOI: 10.1039/c4cp02132k

www.rsc.org/pccp

1. Introduction

Graphene has many exceptional properties and is expected to have several important applications.^{1,2} However, as graphene is a zero gap semiconductor with an inert surface, changing its electronic properties or surface chemistry may be beneficial for particular applications, for example, nanoelectronic devices and sensors. Heteroatomic doping is a powerful way to tailor material properties, with initial studies into demonstrating the capability to alter the electronic properties of graphene.³ In recent years several experimental techniques have been developed to dope the carbon lattice, including *in situ* methods, where doping occurs simultaneously as graphene domains form,^{4–6} and post-production modification techniques.^{7,8} However, comparing results from different laboratories, that were obtained using diverse equipment, and with various growth parameters is difficult if not impossible. Therefore, it is important to conduct detailed and systematic parameter studies using a constant experimental set-up. The influence of individual parameters on

the growth of graphene can then be identified and harnessed to promote desirable properties. Systematic growth studies are therefore fundamentally important before doped CVD graphene can be industrially exploited.

Although heteroatomic doping seems a straightforward way to tune the properties of graphene films, controlled introduction of dopants is challenging. Since bonding of sp²-hybridized carbon atoms in graphene is very strong, substitutional doping (*i.e.*, replacing carbon atoms in a hexagonal lattice with atoms of another element) hardly occurs, except for chemical bonding between dopants and carbon atoms at imperfection sites, such as point defects or edges. Schiros *et al.* have shown that different C–N bond types, including graphitic, pyridinic, and nitrilic, can exist in a single nitrogen-doped graphene sheet and that these bond types have profoundly different effects on the carrier concentration. Consequently, control over the dopant bond type is a crucial requirement in advancing graphene electronics.⁹ The incorporation of nitrogen into the carbon network is energetically unfavourable,¹⁰ and so less doping is likely at high temperatures. For example, increasing the growth temperature from 800 to 900 °C decreased the nitrogen content of carbon nanotubes by half.¹¹ On the other hand, Kidambe *et al.* have shown that the quality of the graphene is compromised at lower growth temperature,¹² even though lower growth temperature would be beneficial to reduce the substrate evaporation and step formation during graphene growth.^{13,14} The temperature also has a significant influence on the graphene

^a Department of Materials, University of Oxford, Oxford, OX1 3PH, UK.
E-mail: nicole.grobert@materials.ox.ac.uk; Tel: +44 1865 283720

^b Institute for Technical Physics and Materials Science, Research Centre for Natural Sciences, PO Box 49, 1525 Budapest, Hungary

^c National Physical Laboratory, Hampton Road, Teddington, Middlesex, TW11 0LW, UK

† Electronic supplementary information (ESI) available. See DOI: 10.1039/c4cp02132k

1 growth rate, which cannot be ignored. Therefore we investigated
the effect of the most important experimental parameters: (i) the
synthesis temperature and (ii) the ammonia concentration on the
growth of nitrogen-doped graphene. This work shows the rela-
5 tionship between these synthesis parameters and the quality,
growth rate, and dopant concentration of nitrogen-doped gra-
phene, allowing the optimum conditions to be identified for the
growth of graphene with desirable properties for use in new
materials for future applications. The incorporation of nitrogen
10 was investigated using Raman spectroscopy, X-ray photoelectron
spectroscopy (XPS), scanning tunneling microscopy (STM) and
current imaging tunneling spectroscopy (CITS).

15 2. Experimental

2.1. Synthesis of nitrogen-doped graphene

Graphene was synthesised by low-pressure chemical vapour
deposition using CH_4 as the carbon source and NH_3 as the
nitrogen source, in the presence of excess H_2 on 25 μm thick Cu
foils (99.999%; Alfa Aesar). The CVD set-up consisted of a
20 quartz tube (20 mm ID) located inside a horizontal cylindrical
furnace and connected to a scroll pump. The Cu substrates
were washed in acetic acid for 10 minutes and placed inside the
quartz tube but kept outside the hot zone of the furnace. The
25 system was evacuated to a base pressure of <0.01 Torr, purged
with Ar, backfilled with 500 sccm H_2 at 3.2 Torr and the furnace
was heated to 1035 $^\circ\text{C}$. The Cu substrates were rapidly heated
by shifting them into the hot zone of the furnace and annealed
at 1035 $^\circ\text{C}$ for 30 minutes using the same H_2 flow. Once the
30 substrates were annealed, the furnace was cooled to the growth
temperature in 20 minutes, and nitrogen-doped graphene was
grown using 5 sccm CH_4 , 0.1–0.5 sccm NH_3 and 100–500 sccm
 H_2 flow for 5–30 min at 900–1000 $^\circ\text{C}$. The reference pristine
(undoped) sample was grown using 5 sccm CH_4 and 500 sccm
35 H_2 flow for 5 min at 1000 $^\circ\text{C}$. Depending on the total gas flow
the pressure changed between 1.3 and 3.3 Torr. After the
growth period the precursor flow was switched off and the
substrates were quenched by rapidly shifting out of the hot
zone to cool in a hydrogen atmosphere.

2.2. Characterisation of the samples

The samples were characterised by scanning electron micro-
scopy (SEM), transmission electron microscopy (TEM), Raman
45 spectroscopy, X-ray photoelectron spectroscopy (XPS) and scan-
ning tunnelling microscopy (STM)/current imaging tunnelling
spectroscopy (CITS). A JEOL JSM-6500F was operated at 5 kV for
SEM imaging. TEM was conducted on a JEOL 2010 TEM
operated at 200 kV. A JY Horiba Labram Raman spectrometer
50 equipped with a 532 nm laser was used to collect Raman data.
Care was taken to use low laser power (<1 mW) in order to
avoid any laser-induced sample damage during the measure-
ments. We observed some fluctuation of the peak position and
intensity ratios on the same sample^{3,15} and so present repre-
55 sentative spectra with peak positions near the average of multi-
ple measurements. XPS measurements were performed using a

Kratos AXIS Ultra DLD with monochromatic Al $\text{K}\alpha$ excitation.
The STM/CITS images were recorded with a Veeco Nanoscope E
in air at 500 pA and 100 mV using Pt90/Ir10 tips on as-grown
samples without transferring from Cu foil. Although contami-
5 nation species were present on the graphene, consecutive
scans of the same area with a small tip-sample distance
removed the physisorbed contamination. Images were recorded
once consecutive scans stabilised and showed no observable
differences.

10 3. Results and discussion

We investigated the effect of the experimental parameters on
the quality and growth rate of nitrogen-doped graphene. A TEM
image of a nitrogen-doped graphene domain and the corres-
ponding electron diffraction pattern characteristic to single-
layer graphene are shown on Fig. S1 (ESI[†]). Bilayer and multi-
15 layer regions were also identified *via* TEM imaging. In order to
achieve uniform incorporation of nitrogen in the graphene
lattice, the nitrogen precursor was introduced simultaneously
with the carbon precursor. Since the incorporation of nitrogen
in graphitic carbon network is more likely at lower tempera-
20 tures¹¹ and nitrogen atoms are less strongly bound to Cu
surfaces than carbon atoms,¹⁶ it is expected that graphene
grown at lower temperature should have higher nitrogen con-
tent. Therefore we investigated the effect of the synthesis
temperature and the ammonia flow rate on the dopant concen-
25 tration, growth rate, nucleation density and coverage of
nitrogen-doped graphene.

We confirmed the nitrogen doping of graphene synthesised
with NH_3 using Raman spectroscopy (Fig. 1). Changes in the
position of the characteristic Raman bands of graphene – the G
peak and 2D peak (also known as G' peak) – indicate n-type
30 doping due to the influence of substitutional nitrogen dopants.¹⁷

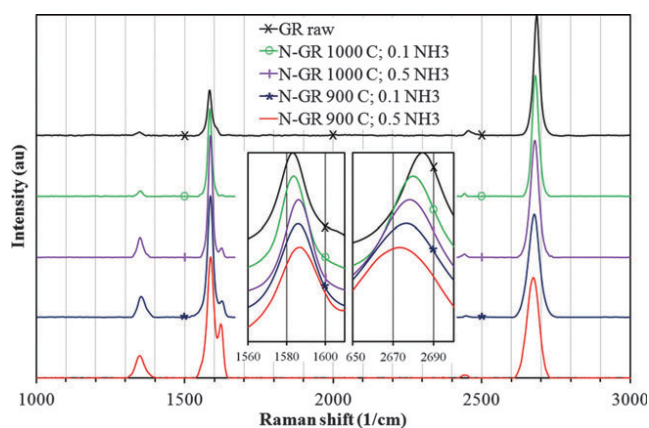


Fig. 1 Representative Raman spectra of nitrogen-doped and raw gra-
45 phene domains on Cu recorded with 532 nm laser. A decrease in the 2D/G
intensity ratio, increase in the D and D' peak intensity, and shift in the
position of the G and 2D peaks (inset) demonstrates the incorporation of
nitrogen dopants. Greater doping is observed for lower synthesis tem-
50 peratures and higher NH_3 flow rates. We observed fluctuation of the peak
positions in the range of 2 cm^{-1} , the figure shows representative spectra
with peak positions near the average of multiple measurements.

1 In addition, heteroatom doped samples typically show a strong D
2 peak, and also exhibit an additional peak at 1620 cm^{-1} (known
3 as the D' band) due to the inter-valley and intra-valley double
4 resonance process in graphene.^{18,19} We compared the position
5 of the G and 2D peaks for graphene samples synthesised using
6 NH_3 with peak positions from a pristine graphene sample that
7 was synthesised under equivalent conditions of 5 sccm CH_4 and
8 500 sccm H_2 at $1000\text{ }^\circ\text{C}$ for 5 minutes. For the pristine graphene
9 the G peak appeared at 1583 cm^{-1} and the 2D peak at 2685 cm^{-1}
10 (Fig. 1). The G peak position was blue-shifted and the 2D peak
11 position was red-shifted for graphene synthesised with NH_3 ,
12 thereby confirming nitrogen doping (Fig. 1).

13 Once nitrogen doping was confirmed, Raman spectroscopy
14 was used to investigate the quality and relative dopant concen-
15 tration of nitrogen-doped graphene synthesised with different
16 NH_3 flow rates (0.1 and 0.5 sccm) and at different synthesis
17 temperatures (900 and $1000\text{ }^\circ\text{C}$). Although a quantitative esti-
18 mate of dopant concentration is possible through the shift of
19 peak positions, this can be misleading.¹⁸ Instead, the relative
20 amount of doping between samples can be inferred by the
21 magnitude of different peak shifts. The intensity of the D and
22 D' peaks also provides some quantitative indication of dopant
23 concentration.

24 Our experiments demonstrate that increasing the NH_3 flow
25 rate from 0.1 sccm to 0.5 sccm resulted in a blue-shift of the G
26 peak, and a red-shift of the 2D peak, suggesting an increase in
27 nitrogen doping (Fig. 1). For instance, when comparing
28 nitrogen-doped graphene produced at $1000\text{ }^\circ\text{C}$ using 0.5 sccm
29 NH_3 with samples synthesised using 0.1 sccm NH_3 , the average
30 2D peak position red-shifted by $\sim 2\text{ cm}^{-1}$ and the average G
31 peak position blue-shifted by $\sim 2\text{ cm}^{-1}$. We therefore conclude
32 that a higher dopant concentration was achieved by increasing
33 the ammonia flow rate.

34 Further studies demonstrate that decreasing the synthesis
35 temperature from $1000\text{ }^\circ\text{C}$ to $900\text{ }^\circ\text{C}$ also resulted in a blue-shift
36 of the G peak position, and a red-shift of the 2D peak position
37 (Fig. 1, comparing green line with blue line, and purple line with
38 red line). For instance, comparing nitrogen-doped graphene
39 produced at $1000\text{ }^\circ\text{C}$ using 0.1 sccm NH_3 with samples synthesised
40 at $900\text{ }^\circ\text{C}$ the average 2D peak position red-shifted by $\sim 4\text{ cm}^{-1}$
41 and the average G peak position blue-shifted by $\sim 2\text{ cm}^{-1}$ (Fig. 1).
42 We therefore conclude that a higher dopant concentration was
43 achieved by reducing the synthesis temperature. This is the first
44 observation demonstrating the importance of synthesis tempera-
45 ture on the dopant concentration of nitrogen-doped graphene,
46 and is in agreement with previous studies on the influence on
47 temperature on the nitrogen-doping of carbon nanotubes.¹¹

48 The magnitude of the shift of Raman peak positions was
49 greater for samples synthesised at lower temperatures (*e.g.*
50 $900\text{ }^\circ\text{C}$ rather than $1000\text{ }^\circ\text{C}$) compared to samples synthesised
51 with higher ammonia flow rates (*e.g.* 0.5 sccm rather than
52 0.1 sccm). For instance, the two samples synthesised at $900\text{ }^\circ\text{C}$,
53 with 0.1 sccm NH_3 and 0.5 NH_3 , have 2D peaks red-shifted
54 $\sim 8\text{ cm}^{-1}$ and $\sim 11\text{ cm}^{-1}$ and G peaks blue-shifted $\sim 3\text{ cm}^{-1}$ and
55 $\sim 4\text{ cm}^{-1}$, respectively, whereas the two samples synthesised at
56 $1000\text{ }^\circ\text{C}$, again with 0.1 NH_3 and 0.5 sccm NH_3 , have 2D peaks

57 red-shifted only $\sim 4\text{ cm}^{-1}$ and $\sim 5\text{ cm}^{-1}$ and G peaks blue-
58 shifted only $\sim 1\text{ cm}^{-1}$ and $\sim 3\text{ cm}^{-1}$, respectively. The synthesis
59 temperature therefore has a greater influence on the peak shift
60 (and hence nitrogen dopant concentration), rather than the NH_3
61 flow rate as one might be expected. In other words, reducing the
62 synthesis temperature by $100\text{ }^\circ\text{C}$ results in a greater increase in
63 nitrogen doping than a five times increase in NH_3 flow rate. We
64 therefore conclude that the synthesis temperature is an over-
65 riding parameter for controlling the concentration of nitrogen-
66 doped graphene. This observation has important implications if
67 manufacturers are to maximise the concentration of nitrogen-
68 doped graphene while reducing production costs.

69 From the Raman spectra in Fig. 1, an increase of the
70 intensity of the D peak and the D' peak is concurrently observed
71 for increasing nitrogen-doping of the sample. For instance, an
72 increase in D and D' peak intensity is observed between
73 samples synthesised at $1000\text{ }^\circ\text{C}$ with 0.1 sccm NH_3 and 0.5 sccm
74 NH_3 , and this trend continues for samples synthesised at
75 $900\text{ }^\circ\text{C}$ with 0.1 sccm and 0.5 sccm NH_3 (Fig. 1). The increase
76 in the disorder in the graphene lattice with increased nitrogen-
77 doping also results in a decrease in the 2D peak intensity. This
78 is due to the fact that increased disorder in the lattice decreases
79 the probability of two phonon scattering required to generate
80 the 2D peak.²⁰

81 Based on the Raman spectroscopy the nitrogen content of
82 the graphene domains produced at lower temperatures and
83 higher NH_3 flow rate are expected to have the highest nitrogen
84 concentration. Therefore, we conducted complementary XPS
85 analysis of nitrogen-doped graphene synthesised at $900\text{ }^\circ\text{C}$ with
86 0.5 sccm NH_3 , (Fig. 2) to determine the maximum concen-
87 tration and bonding configuration of N in the samples. XPS
88 measurements were performed both before and after a $300\text{ }^\circ\text{C}$
89 anneal in UHV (Fig. 2a, c, e, and Fig. 2b, d, f, respectively). C 1s
90 peaks detected at $\sim 284.4\text{ eV}$ and $\sim 285.0\text{ eV}$ (Fig. 2a and b)
91 correspond to graphite-like sp^2 -hybridised carbon and other
92 hydrocarbon species respectively. The sp^2 -hybridised carbon
93 peak is typical for graphene surfaces but also for other carbon
94 contaminants as well, two peaks at $\sim 288.3\text{ eV}$ and $\sim 286.4\text{ eV}$
95 are also observed and nominally assigned as acid ester and
96 alcohol groups respectively.²¹ These peaks are associated with
97 contaminants on the surface that have been adsorbed whilst
98 the sample was in ambient conditions. These peaks also coin-
99 cide with the O 1s peak observed in Fig. 2c and d at $\sim 531.7\text{ eV}$,
100 which is attributed to oxygen-bound carbon species. This peak
101 is also related to copper hydroxide,²² as elemental analysis
102 shows that this peak cannot be solely due to carbon contami-
103 nants. A copper oxide peak is also observed in the O 1s spectra
104 at $\sim 530.3\text{ eV}$.

105 The comparative spectra in Fig. 2a and b therefore show a
106 reduction in carbon contaminants after the annealing process.
107 The peaks associated with acid ester and alcohol groups are
108 shown to decrease, as do the peaks associated with hydrocar-
109 bons. The peak in the O 1s spectra associated with organic
110 species also reduces significantly, as expected.

111 The XPS spectra in Fig. 2e and f relate to the nitrogen
112 content in the sample. Two distinct peaks are visible even with

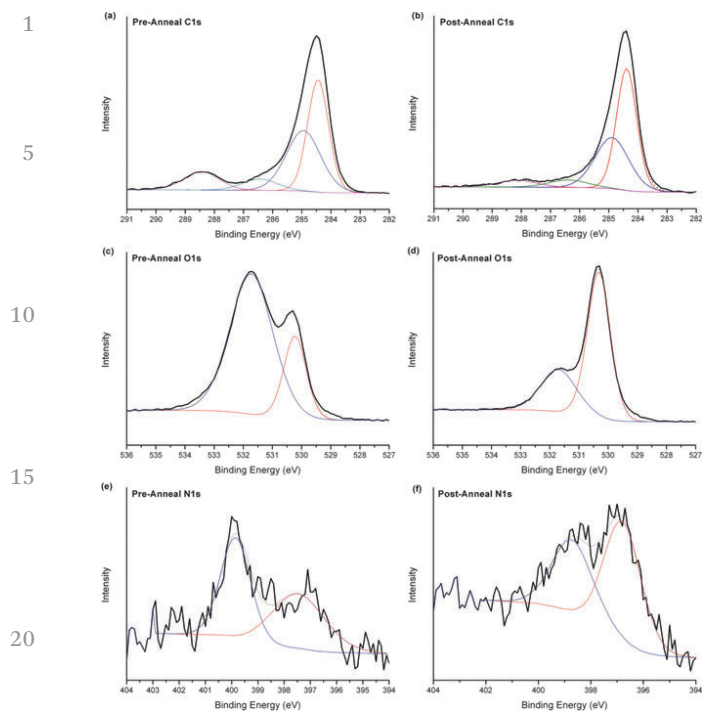


Fig. 2 XPS spectra for nitrogen-doped graphene synthesised with 5 sccm CH_4 and 0.5 sccm NH_3 at 900 °C. XPS obtained on a copper substrate before (a, c, e) and after (b, d, f) the sample was annealed at 300 °C for 30 min in UHV, with the associated C 1s (a and b), O 1s (c and d) and N 1s (e and f) peak-fitted spectra.

a low signal due to the proportionally small amount of nitrogen present in the surface. These two peaks relate to carbon-bound nitrogen and copper nitride species in the sample, with peak positions of $\sim 398.7\text{--}399.8$ eV and $\sim 396.8\text{--}397.5$ eV respectively. After annealing the amount of nitrogen associated with carbon is still approximately the same, however, the proportion of copper nitride present in the sample increases and appears to be distributed deeper in the sample due to the rise in background on the high binding energy side of the peak caused by inelastically scattered electrons. Although separate peaks are not fitted for pyridinic and pyrrolic conformations due to the low signal-to-noise ratio and the large uncertainty in the peak positions from literature,²³ a shift from 399.8 eV to 398.7 eV is observed for the C–N peak after the sample is heated, indicating a reduction in pyrrolic species as the contamination on the surface is reduced, and an increase in the ratio of pyridinic/pyrrolic species present. There is no peak wholly attributed to amide species in the C 1s spectra due to the larger percentage of carbon–oxygen species obviously present.

By comparing the C 1s peaks – that are associated with graphene (and other sp^2 -hybridised carbon) – with the N 1s peak – associated with carbon-bound nitrogen after the annealing process – we can suggest that the more heavily nitrogen-doped graphene sample has a nitrogen content of *ca.* 2.1% overall. However, the true percentage of nitrogen present in the graphene could only be determined if there was no adsorbed contamination still present after the annealing process. For comparison, an undoped graphene sample that was prepared

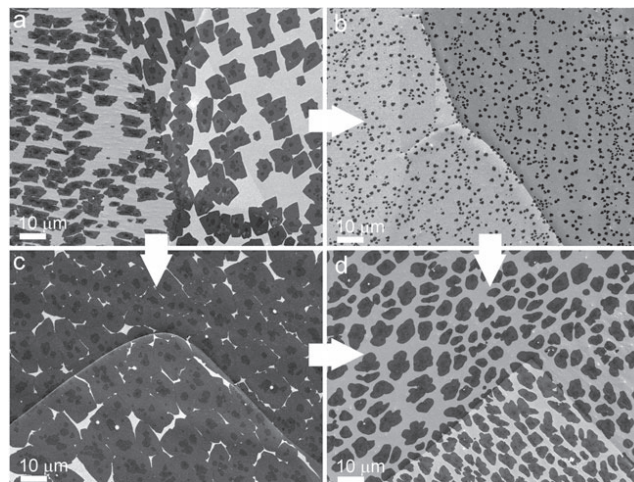


Fig. 3 SEM images of graphene domains on Cu. (a) Sample grown at 1000 °C with 0.1 sccm NH_3 , 5 sccm CH_4 and 500 sccm H_2 in 5 min, with growth rate of ~ 1.58 $\mu\text{m min}^{-1}$; (b) decrease of growth temperature to 900 °C decreased the growth rate of the nitrogen-doped graphene domains significantly to ~ 0.34 $\mu\text{m min}^{-1}$; (c) nearly full coverage for sample grown at 1000 °C with 0.5 sccm NH_3 in 10 min, but equivalent to a reduced growth rate of only 1.34 $\mu\text{m min}^{-1}$ due to increased NH_3 flow; (d) incomplete maximum surface coverage at 900 °C with 0.5 NH_3 and 100 H_2 in 30 min.

using the same procedure, but without any NH_3 exposure, was found to have a carbon-bound nitrogen content of 0.8% due to adventitious contamination, present because of unavoidable exposure to ambient conditions before XPS analysis.

To investigate the influence of the synthesis parameters on the growth rate of nitrogen-doped graphene experiments were stopped before the copper substrate was fully covered by graphene domains. Domain sizes were then compared *via* SEM imaging (Fig. 3). Our experiments demonstrate that decreasing the synthesis temperature and increasing the ammonia flow reduces the growth rate of nitrogen-doped graphene. With respect to the influence of temperature, the average graphene domain size was ~ 7.9 μm at 1000 °C (Fig. 3a), but only ~ 1.7 μm at 900 °C (Fig. 3b) when using 5 sccm CH_4 , 0.1 sccm NH_3 and 500 sccm H_2 for 5 minutes. This equates to a growth rate of 1.58 $\mu\text{m min}^{-1}$ at 1000 °C, which decreased nearly three times to 0.54 $\mu\text{m min}^{-1}$ at 950 °C, and further decreased to 0.34 $\mu\text{m min}^{-1}$ at 900 °C (Fig. 4). These observations follow a similar trend to previous studies into the influence of synthesis temperature on the growth rate of pristine graphene.²⁴ Increasing the NH_3 flow also decreased the growth rate, and as a consequence it was necessary to increase the duration of experiments and/or decrease the hydrogen flow so that domains were of an appreciable size for SEM imaging. This change in time and hydrogen concentration helped to grow larger graphene domains without influencing their quality, and provides the opportunity for comparing the growth rate between experiments with different NH_3 flow. For example, at 1000 °C using 5 sccm CH_4 , 0.5 sccm NH_3 and 500 sccm H_2 for 10 minutes resulted in average domain size of 13.4 μm (Fig. 3c). Comparing this growth with Fig. 3a, a five times increase of ammonia concentration (from 0.1 sccm to 0.5 sccm) decreased the average

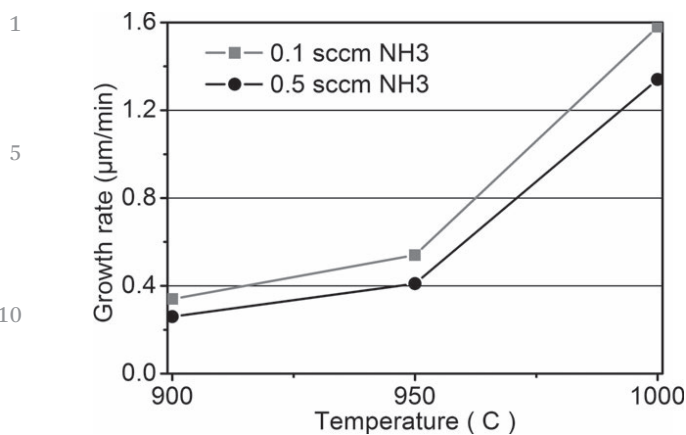


Fig. 4 Influence of the temperature and ammonia concentration on the average graphene growth rate. The temperature caused significant change, while the effect of ammonia concentration appeared less important.

growth rate by approximately 15% (from $1.58 \mu\text{m min}^{-1}$ to $1.34 \mu\text{m min}^{-1}$). At lower temperatures, 950 and 900 °C, a similar increase in ammonia concentration decreased the average growth rate approximately 25% (Fig. 4). Therefore, production of nitrogen-doped graphene at 900 °C using 5 sccm CH₄ and 0.5 sccm NH₃ required extended synthesis times (e.g. 30 minutes) and reduced H₂ flow rates (e.g. 100 sccm H₂) (Fig. 3d). Collectively, we conclude that a decrease in synthesis temperature and increase of ammonia concentration caused a significant decrease in the growth rate of nitrogen-doped graphene (e.g. 100 °C reduction and five times increase in NH₃ flow rate resulted in approximately six times decrease in $\mu\text{m min}^{-1}$ coverage) (Fig. 4).

The temperature and ammonia concentration also influenced the graphene nucleation density and the maximum achievable surface coverage. Full coverage (or nearly full coverage) was observed when using high temperatures and high ammonia concentrations, i.e. 1000 °C; 0.5 sccm NH₃; 500 sccm H₂; 10 min (Fig. 3c), or low temperatures and low ammonia concentrations, i.e. 900 °C; 0.1 sccm NH₃. However, only half of the copper substrate was covered at low temperatures and high ammonia concentrations, i.e. 900 °C; 0.5 sccm NH₃. Even for experiments with reduced H₂ flow rate (to minimise etching of domains) and extended synthesis time (e.g. 30 minutes or longer) the size of the graphene domains did not increase significantly (Fig. 3d), meaning only incomplete maximum surface coverage is achievable under such conditions. We believe this is due to the ammonia damaging the copper surface and inhibiting the growth of domains. Consequently, using the right balance between the experimental parameters, it is possible to tune the surface coverage and growth rate of nitrogen-doped graphene. These findings have important implications for optimising the sample quality while minimising the production time and associated costs of manufacturing nitrogen-doped graphene if this material is to become viable for commercial applications in the future.

A typical lower resolution STM image of the nitrogen-doped graphene synthesised at 900 °C with 0.5 sccm NH₃ is shown in Fig. 5a. STM measurements found that there was physisorbed

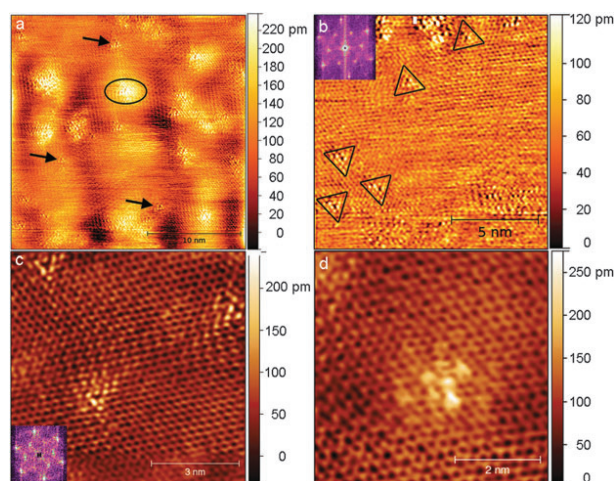


Fig. 5 (a) Lower resolution STM image of nitrogen-doped graphene showing substitutional nitrogen atoms (arrows)²⁵ and larger defects likely containing multiple nitrogen atoms (oval). (b) Higher resolution STM image revealing typical patterns around individual substitutional nitrogen atoms oriented differently on different sublattices as highlighted by triangles. The inset presents the FFT of the STM image: the outer hexagon corresponds to the atomic lattice, the inner hexagon arises from the intervalley scattering induced by nitrogen dopants. (c) Additional examples of nitrogen atoms (d) a defect resembling the pyridinic configuration.²⁹

contamination present on the surface after exposure to ambient conditions (not shown), as observed with XPS. Comparison of the STM images with computer simulations revealed that the nitrogen was incorporated mainly in substitutional configuration. Several larger defects likely containing more than one nitrogen atom were also observed (circled in Fig. 5a). Similar STM studies of pristine, undoped graphene did not reveal any substitutional nitrogen. Higher resolution STM imaging of nitrogen-doped graphene shows rotated patterns (highlighted with triangles in Fig. 5b) indicating substitutional nitrogen atoms are incorporated on different graphene sublattices. The STM image shows good correspondence with the DFT calculations reported by Lambin *et al.*²⁵ The substitutional nitrogen incorporation was also confirmed by STEM and EELS investigation of the nitrogen-doped graphene samples.²⁶ During STEM/EELS measurement only substitutional nitrogen atoms were identified, which indicates that the concentration of other types of nitrogen atoms was low. The fast Fourier transform (FFT) of Fig. 5b (inset) shows two sets of points arranged in hexagons. The outer hexagon corresponds to the atomic lattice, while the inner hexagon shows intervalley scattering induced by nitrogen dopants.^{3,27} These strong intervalley peaks caused by electron scattering processes between two non-equivalent Dirac cones²⁸ indicate a significant influence of the nitrogen atoms on the electronic properties of the graphene. This observation is in agreement with the increase in intervalley scattering detected by the increased I_D/I_G ratio in the Raman spectra. Additionally, defects resembling the pyridinic configuration²⁹ were also observed (Fig. 5d).

We investigated the effect of nitrogen on the density of states of nitrogen-doped graphene using CITS. Fig. 6a shows an atomic resolution STM image with nitrogen atoms

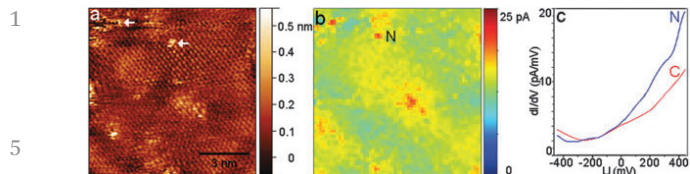


Fig. 6 (a) STM image of nitrogen-doped graphene domain. (b) Corresponding CITS image at 335 mV. A minor translational shift exists between the STM in (a) and CITS image. (c) dI/dV recorded above a nitrogen atom (marked N on image b) and a carbon atom.

incorporated in the graphene lattice. The localized high current regions on the CITS image (Fig. 6b) correspond to substitutional nitrogen atoms (indicated by arrows Fig. 6a, with minor translational shift). The diffuse maxima are due to the defects containing more than one nitrogen atom, as observed in STM. The measurements show that the electronic structure of nitrogen-doped graphene was strongly modified only within a few lattice spacing of the site of the nitrogen. The minimum of the dI/dV curve measured above the substitutional nitrogen atom marked by letter 'N' was near -300 meV (Fig. 6c), similar to other measurements reported in literature.³ This suggests the nitrogen-doped graphene displays n-type doping, in agreement with our Raman measurements. Local densities of states above the Fermi level around nitrogen atoms increased dI/dV at positive voltages as it could be expected from DFT calculations.²⁵

4. Conclusions

We investigated the effect of the experimental parameters on the growth of nitrogen-doped graphene produced by LPCVD and doped *in situ* during growth using NH_3 . STM imaging confirmed that nitrogen was incorporated mainly in substitutional configuration, while CITS demonstrated that the nitrogen-doped graphene has n-type doping. We showed that the synthesis parameters influence the dopant concentration and growth rate of nitrogen-doped graphene. Raman spectroscopy demonstrated that reducing the synthesis temperature and increasing the NH_3 flow rates increased the concentration of nitrogen dopants. Our results demonstrate that the synthesis temperature, not NH_3 flow rate, is the overriding parameter, as a 100 °C decrease in temperature increased the concentration of nitrogen dopants more than a five times increase in NH_3 flow rate. XPS analysis showed that the highest overall nitrogen concentration was approximately 2.1%, achievable by using a lower synthesis temperature (900 °C) and higher NH_3 flow rate (0.5 sccm). However, decreasing the temperature and increasing the NH_3 flow rate also significantly decreased the growth rate of nitrogen-doped graphene. Furthermore, under particular conditions that would maximise nitrogen doping – using low synthesis temperatures (e.g. 900 °C) and high NH_3 flow rate (e.g. 0.5 sccm, or above) – the growth of nitrogen-doped graphene was inhibited so that full coverage of the Cu surface was not possible even with extended synthesis time. Therefore the right balance between the nitrogen content and growth rate must be found, and consequently accurate optimisation is needed to produce high quality nitrogen-doped graphene.

These findings have important implications for optimising the dopant concentration and sample quality, while minimising the production time and associated costs, if nitrogen-doped graphene is to find commercial applications in the future.

Acknowledgements

We are grateful to the European Research Council (ERC-2009-StG-240500) (N. G.), the Royal Society (N. G.), the Engineering and Physical Sciences Research Council Pathways to Impact Awards (N. G.), the Commonwealth Scholarship Commission (A. T. M.), University of Oxford Clarendon Fund (A. T. M.), OTKA K 101599 (N. I. P., B. L. P.), and the National Measurement Office through the Innovation Research and Development Programme (A.J.P., S.J.S., A.G.S., D.R.) for financial support.

Notes and references

- 1 A. K. Geim and K. S. Novoselov, *Nat. Mater.*, 2007, **6**, 183.
- 2 A. K. Geim, *Science*, 2009, **324**, 1530.
- 3 L. Zhao, R. He, K. T. Rim, T. Schiros, K. S. Kim and H. Zhou, *et al*, *Science*, 2011, **333**, 999.
- 4 D. Wei, Y. Liu, Y. Wang, H. Zhang, L. Huang and G. Yu, *Nano Lett.*, 2009, **9**, 1752.
- 5 L. S. Panchakarla, K. S. Subrahmanyam, S. K. Saha, A. Govindaraj, H. R. Krishnamurthy and U. V. Waghmare, *et al.*, *Adv. Mater.*, 2009, **21**, 4726.
- 6 Z. Sun, Z. Yan, J. Yao, E. Beitler, Y. Zhu and J. M. Tour, *Nature*, 2010, **468**, 549.
- 7 X. Wang, X. Li, L. Zhang, Y. Yoon, P. K. Weber and H. Wang, *et al.*, *Science*, 2009, **324**, 768.
- 8 Y. C. Lin, C. Y. Lin and P. W. Chiu, *Appl. Phys. Lett.*, 2010, **96**, 133110.
- 9 T. Schiros, D. Nordlund, L. Palova, D. Prezzi, L. Zhao and K. S. Kim, *et al.*, *Nano Lett.*, 2012, **12**, 4025.
- 10 E. Cruz-Silva, F. Lopez-Urias, E. Munoz-Sandoval, B. G. Sumpter, H. Terrones and J. C. Charlier, *et al*, *ACS Nano*, 2009, **3**, 1913.
- 11 A. A. Koos, M. Dowling, K. Jurkschat, A. Crossley and N. Grobert, *Carbon*, 2009, **47**, 30.
- 12 P. R. Kidambi, C. Ducati, B. Dlubak, D. Gardiner, R. S. Weatherup and M. B. Martin, *et al*, *J. Phys. Chem. C*, 2012, **116**, 22492.
- 13 A. T. Murdock, A. A. Koos, T. B. Britton, L. Houben, T. Batten and T. Zhang, *et al*, *ACS Nano*, 2013, **7**, 1351.
- 14 K. Kertesz, A. A. Koos, A. T. Murdock, Z. Vertesy, P. Nemes-Incze and P. J. Szabo, *et al*, *Appl. Phys. Lett.*, 2012, **100**, 213103.
- 15 Z. Zafar, Z. H. Ni, X. Wu, Z. X. Shi, H. Y. Nan, J. Bai and L. T. Sun, *Carbon*, 2013, **61**, 57.
- 16 X. Y. Pang, L. Q. Xue and G. C. Wang, *Langmuir*, 2007, **23**, 4910.
- 17 M. Kalbac, A. Reina-Cecco, H. Farhat, J. Kong, L. Kavan and M. S. Dresselhaus, *ACS Nano*, 2010, **4**, 6055.
- 18 R. Podila, J. Chacon-Torres, J. T. Spear, T. Pichler, P. Ayala and A. M. Rao, *Appl. Phys. Lett.*, 2012, **101**, 123108.

- 1 19 L. G. Cancado, M. A. Pimenta, B. R. A. Neves, M. S. S. Dantas and A. Jorio, *Phys. Rev. Lett.*, 2004, **93**, 247401.
- 20 E. H. M. Ferreira, M. V. O. Moutinho, F. Stavale, M. M. Lucchese, R. B. Capaz and C. A. Achete, *et al*, *Phys. Rev. B: Condens. Matter Mater. Phys.*, 2010, **82**, 125429.
- 5 21 J. C. Vickerman and I. S. Gilmore, *Surface Analysis – The Principal Techniques*, 2nd edn, Wiley, 2009.
- 22 J. F. Moulder, W. F. Stickle, P. E. Sobol and K. D. Bomben, *Handbook of X-ray photoelectron spectroscopy*, Perkin-Elmer Corp., 1992.
- 10 23 W. J. Gammon, O. Kraft, A. C. Reilly and B. C. Holloway, *Carbon*, 2003, **41**, 1917.
- 24 S. Xing, W. Wu, Y. Wang, J. Bao and S. S. Pei, *Chem. Phys. Lett.*, 2013, **580**, 62–66.
- 25 Ph. Lambin, H. Amara, F. Ducastelle and L. Henrard, *Phys. Rev. B: Condens. Matter Mater. Phys.*, 2012, **86**, 045448.
- 26 R. J. Nicholls, A. T. Murdock, J. Tsang, J. Britton, T. J. Pennycook and A. Koós, *et al*, *ACS Nano*, 2013, **7**, 7145.
- 5 27 G. M. Rutter, J. N. Crain, N. P. Guisinger, T. Li, P. N. First and J. A. Stroscio, *Science*, 2007, **317**, 219.
- 28 I. Brihuega, P. Mallet, C. Bena, S. Bose, C. Michaelis and L. Vitali, *et al*, *Phys. Rev. Lett.*, 2008, **101**, 206802.
- 10 29 B. Zheng, P. Hermet and L. Henrard, *ACS Nano*, 2010, **4**, 4165.
- 15
- 15
- 20
- 20
- 25
- 25
- 30
- 30
- 35
- 35
- 40
- 40
- 45
- 45
- 50
- 50
- 55
- 55